Application of a multiregion model to the EM scattering from a rough surface with or without a target above it*

Wang An-Qi(王安琪)†, Guo Li-Xin(郭立新), and Chai Cao(柴 草)

School of Science, Xidian University, Xi'an 710071, *China*

(Received 17 June 2010; revised manuscript received 17 January 2011)

An efficient multiregion model is introduced to calculate the electromagnetic scattering from a perfectly electrical conducting (PEC) rough surface with or without a PEC target above it. In the multiregion model, the rough surface is split into multiple regions depending on their position along the rough surface. Two intermediate regions are chosen as the dominant region. If a target is located above the rough surface, the target will also be included in the dominant region. The method of moments (MOM) is only adopted on the dominant region to ensure validity. Hence, the new model can greatly reduce the number of unknowns associated with full MOM analysis. The induced electric currents on the other regions are obtained by approximately considering the mutual coupling between different regions along the rough surface. Compared with the published hybrid method, this new model is not only suitable for EM scattering from a target above a rough surface but also applicable for just rough surfaces. Several numerical simulations are presented to show the validity and efficiency of the multiregion model.

Keywords: multiregion model, electromagnetic scattering, rough surface, method of moments

PACS: 02.60.Jh, 41.20.Jb, 43.30.Hw **DOI:** 10.1088/1674-1056/20/5/050201

1. Introduction

Electromagnetic (EM) scattering from a rough surface with or without a target has been extensively investigated during recent years for a large number of applications in radar surveillance, target tracking and oceanic remote sensing.[1−3] Several kinds of method, including analytical and numerical methods, have been applied to solve this scattering problem. However, methods based on the approximate analytical method[4,5] have strict limitations, low precision and are too weak to calculate the composite scattering from a rough surface with a target above it. Numerical methods based on Maxwell's equations are generally more applicable and have been widely used to calculate the EM scattering from rough surface and target.[6−11] Among these numerical methods, the method of moments (MOM) is the most popular due to the high accuracy obtained by directly using the boundary conditions on the interfaces.[7−11] Unfortunately, the conventional MOM needs $O(N^2)$ system memory and $O(N^2)$ computational time for each iterated process, which is very expensive when the number of unknowns N is very large. These issues motivate the development of faster algorithms with which to solve this problem, such as the banded matrix iterative approach/ canonical grid method (BMIA/CAG),[9] the generalized forward backward method with the spectrum acceleration algorithm (GFBM/SAA)[10] and the multilevel sparse matrix canonical grid method (MSMCG).[11] In addition, we propose the parallel MOM to study the properties of EM scattering from a target above a large-scale rough surface under large incidence,[7] and EM-beam scattering from a two-dimensional rough surface.[1,12] Unlike these fast algorithms, based on our previous work,[12−14] the efficient multiregion model[15] is introduced in this work. Because the amplitude of the incident tapered plane wave[4] is Gaussian in the plane $z = 0$ and decays rapidly for $|x| > g$,[16] the induced electric current at the edge of the rough surface is much smaller than that in the center. To perform the multiregion model, the rough surface is split into multiple regions along the rough surface. The two intermediate regions are chosen as the dominant region. The minimum width of the dominant region should be at least the length of g. If a target is located above the rough surface, the target will be also included in

*Project supported by the National Natural Science Foundation of China (Grant No. 60971067), the Specialized Research Fund for the Doctoral Program of Higher Education, China (Grant No. 20100203110016), and the Fundamental Research Funds for the Central Universities, China (Grant No. K50510070001).

†Corresponding author. E-mail: wanganqi0006@163.com

© 2011 Chinese Physical Society and IOP Publishing Ltd

the dominant region. The MOM is only adopted on the dominant region in order to ensure the accuracy of the approach. Hence, the new model can greatly reduce the number of unknowns of the full MOM. If the multiregion model is combined with the fast algorithms mentioned above, efficiency can be greatly improved.

In the previously published literature, the MOM has been combined with the Kirchhoff approximation (KA) to reduce the number of unknowns in calculating the EM scattering from a target located above a rough surface.[13,17] In Ref. [17], the electric field integral equation (EFIE) in the target region is firstly solved by the MOM. Fields on the rough surface are derived through the KA method. Then an iterative approach is utilized by considering interactions between the target and the rough surface. Moreover, we propose a hybrid method (MOM-KA) for investigating composite scattering from a target above a rough surface.[13] Overall, these hybrid methods depend on interactions between the target and the rough surface. In this study, the induced electric currents are obtained by approximately considering the mutual coupling between different regions along the rough surface. Therefore, the multiregion model is not only suitable for EM scattering from a target above a rough surface but also applicable for just rough surfaces. The validity of this approach has been shown by comparing it with the full MOM. Both the distribution of the induced electric current along the rough surface and the scattering pattern of the bistatic scattering coefficient (BSC) over the whole scattering angle have been presented in the numerical simulations.

The reminder of this paper is organized as follows: In Section 2, theoretical formulations of the multiregion model for calculating EM scattering from a rough surface with or without a target above it are derived in detail. Both the horizontal (HH) and vertical (VV) polarizations are considered. Several numerical simulations are presented in Section 3 to show the validity and efficiency of the new model by comparing it with the full MOM. The paper ends in Section 4 with a summary of this new model and a proposition about further investigations.

2. Theoretical formulations of the multiregion model

As shown in Fig. 1 an incident tapered plane wave[4] impinges upon a perfectly electrical conducting (PEC) rough surface with or without a PEC target above it, where $f(x)$ is a Gaussian distributed rough surface, with correlation length l and root mean square (rms) height δ.[4] In this work, the time dependence is $\mathrm{e}^{-\mathrm{i}\,\omega t}$ and the position vector is $\boldsymbol{r} = x\hat{\boldsymbol{x}} + z\hat{\boldsymbol{z}}$.

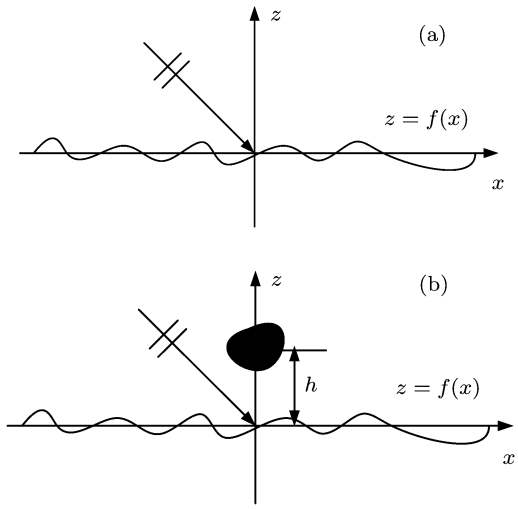


Fig. 1. Geometric models for EM scattering from a rough surface with and without a target above it. (a) Without a target, (b) with a target.

For the HH polarized incidence, the EFIE for calculating the EM scattering from the geometric models of Fig. 1 is defined as[18]

$$\hat{\boldsymbol{t}} \cdot (\boldsymbol{E}^{\mathrm{inc}} + \boldsymbol{E}^{\mathrm{sca}}) = 0, \tag{1}$$

where $\boldsymbol{E}^{\mathrm{inc}}$ and $\boldsymbol{E}^{\mathrm{sca}}$ are the incident and scattered electric fields, respectively; $\hat{\boldsymbol{t}}$ represents the unit tangential vector of the rough surface or target.

For the VV polarized incidence, the magnetic field integral equation (MFIE) is[18]

$$\hat{\boldsymbol{n}} \times (\boldsymbol{H}^{\mathrm{inc}} + \boldsymbol{H}^{\mathrm{sca}}) = \boldsymbol{J}, \tag{2}$$

where $\boldsymbol{H}^{\mathrm{inc}}$ and $\boldsymbol{H}^{\mathrm{sca}}$ are the incident and scattered magnetic fields, $\boldsymbol{J}$ is the induced electric current on the rough surface or target, and $\hat{\boldsymbol{n}}$ indicates the unit normal vector. Moreover, $\hat{\boldsymbol{t}}$, $\hat{\boldsymbol{n}}$ and $\hat{\boldsymbol{y}}$ form a right-handed system.

Because the amplitude of the incident tapered plane wave[4] is Gaussian in the plane $z = 0$ and decays rapidly for $|x| > g$,[16] the amplitude of the incident tapered plane wave is larger in the center of the rough surface than that in the edge regions, the induced electric current in the center of the rough surface is greater than that in the edge regions. When the rough surface is two-dimensional (2D), the Gaussian beam[19] which has a Gaussian shape with half-width W centered at $\boldsymbol{r}_{\mathrm{s}} = \boldsymbol{0}$ in the $z = 0$ plane is chosen

as the incident wave. In other words, the strength of the incident Gaussian beam for the 2D rough surface decays with $|\boldsymbol{r}|$ increasing. The induced currents in the center of the 2D rough surface are also larger than that in the other regions. To perform the multiregion model, the rough surface, including 1D and 2D rough surfaces, is split into multiple regions $S_{1_\mathrm{l}}, S_{1_\mathrm{r}}, S_{2_\mathrm{l}}, S_{2_\mathrm{r}}, \ldots, S_{M_\mathrm{l}}, S_{M_\mathrm{r}}$, and $S_{1_\mathrm{l}} + S_{1_\mathrm{r}} + S_{2_\mathrm{l}} + S_{2_\mathrm{r}} + \cdots + S_{M_\mathrm{l}} + S_{M_\mathrm{r}} = S_\mathrm{s}$ (see Fig. 2). It is necessary to note that in the subscripts s is surface, l indicates left and r represents right. They are the same for the following variables. The two intermediate regions S_{1_l} and S_{1_r} are chosen as the dominant region and handled by the MOM. In addition, the minimum width of the dominant region is at least the length of g. That is, $S_{1_\mathrm{l}} \geq g/2$ and $S_{1_\mathrm{r}} \geq g/2$. Then the amplitude of the incident taper wave satisfies $|\psi^{\mathrm{inc}}(\boldsymbol{r})|_{z=0} \leq \mathrm{e}^{-1/4}$ in the edge of the dominant region. If a target S_o is located above the rough surface, the target will be also included in the dominant region.

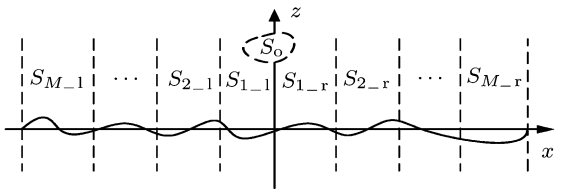


Fig. 2. Configuration of splitting the rough surface into multiple regions.

The induced electric currents along the rough surface are defined as $\boldsymbol{J}_{1_\mathrm{l}}$, $\boldsymbol{J}_{1_\mathrm{r}}$, $\boldsymbol{J}_{2_\mathrm{l}}$, $\boldsymbol{J}_{2_\mathrm{r}}, \ldots,$ $\boldsymbol{J}_{M_\mathrm{l}}$, $\boldsymbol{J}_{M_\mathrm{r}}$ corresponding to regions $S_{1_\mathrm{l}}, S_{1_\mathrm{r}}$, $S_{2_\mathrm{l}}, S_{2_\mathrm{r}}, \ldots,$ $S_{M_\mathrm{l}}, S_{M_\mathrm{r}}$, respectively. Then the scattered electric and magnetic fields can be expressed as

$$\boldsymbol{E}_m^{\mathrm{sca}} = \sum_{p=1}^{M} \bar{\boldsymbol{L}}_\mathrm{E}^{mp_\mathrm{l}} \cdot \boldsymbol{J}_{p_\mathrm{l}} + \sum_{p=1}^{M} \bar{\boldsymbol{L}}_\mathrm{E}^{mp_\mathrm{r}} \cdot \boldsymbol{J}_{p_\mathrm{r}}, \quad (3)$$

$$\boldsymbol{H}_m^{\mathrm{sca}} = \sum_{p=1}^{M} \bar{\boldsymbol{L}}_\mathrm{H}^{mp_\mathrm{l}} \cdot \boldsymbol{J}_{p_\mathrm{l}} + \sum_{p=1}^{M} \bar{\boldsymbol{L}}_\mathrm{H}^{mp_\mathrm{r}} \cdot \boldsymbol{J}_{p_\mathrm{r}}, \quad (4)$$

where $m = 1_\mathrm{l}, 1_\mathrm{r}, 2_\mathrm{l}, 2_\mathrm{r}, \ldots, M_\mathrm{l}, M_\mathrm{r}$, corresponding to regions S_{1_l}, S_{1_r}, S_{2_l}, $S_{2_\mathrm{r}}, \ldots,$ S_{M_l}, S_{M_r}. The operators $\bar{\boldsymbol{L}}_\mathrm{E}^{mn} \cdot \boldsymbol{J}_n$ and $\bar{L}_\mathrm{H}^{mn} \cdot \boldsymbol{J}_n$ in the HH polarization are

$$\bar{\boldsymbol{L}}_\mathrm{E}^{mn} \cdot \boldsymbol{J}_n = \mathrm{i}\,\omega\mu_0 \int_{S_n} G(\boldsymbol{r}, \boldsymbol{r}')\boldsymbol{J}(\boldsymbol{r}')\mathrm{d}S', \quad (5)$$

$$\bar{\boldsymbol{L}}_\mathrm{H}^{mn} \cdot \boldsymbol{J}_n = \nabla \times \int_{S_n} G(\boldsymbol{r}, \boldsymbol{r}')\boldsymbol{J}(\boldsymbol{r}')\mathrm{d}S', \quad (6)$$

where $G(\boldsymbol{r}, \boldsymbol{r}') = \frac{\mathrm{i}}{4} H_0^{(1)}(k_0 |\boldsymbol{r} - \boldsymbol{r}'|)$ is the two-dimensional Green's function,[16] k_0 is the wave number in the free space, and $H_0^{(1)}(\cdot)$ is the zeroth-order Hankel function of the first kind. For VV polarization the operator $\bar{\boldsymbol{L}}_\mathrm{H}^{mn} \cdot \boldsymbol{J}_n$ is also defined as Eq. (6).

Similar to the rule of division presented in Ref. [15], the regions S_{2_l} and S_{2_r}, which are the close neighbors of the MOM region, are firstly considered. Exact solutions of $\boldsymbol{J}_{2_\mathrm{l}}$ and $\boldsymbol{J}_{2_\mathrm{r}}$ can be acquired by Eq. (2). In the multiregion model, they are approximately obtained as follows:

$$\boldsymbol{J}_{2_\mathrm{l}}(\boldsymbol{r}) = 2\hat{\boldsymbol{n}} \times \boldsymbol{H}_{2_\mathrm{l}}^{\mathrm{inc}}(\boldsymbol{r}) + 2\hat{\boldsymbol{n}} \times \bar{\boldsymbol{L}}_\mathrm{H}^{2_\mathrm{l}1_\mathrm{l}} \cdot \boldsymbol{J}_{1_\mathrm{l}}, \quad (7)$$

$$\boldsymbol{J}_{2_\mathrm{r}}(\boldsymbol{r}) = 2\hat{\boldsymbol{n}} \times \boldsymbol{H}_{2_\mathrm{r}}^{\mathrm{inc}}(\boldsymbol{r}) + 2\hat{\boldsymbol{n}} \times \bar{\boldsymbol{L}}_\mathrm{H}^{2_\mathrm{r}1_\mathrm{r}} \cdot \boldsymbol{J}_{1_\mathrm{r}}. \quad (8)$$

Here, the main contribution of $\boldsymbol{J}_{2_\mathrm{l}}$ and $\boldsymbol{J}_{2_\mathrm{r}}$ is evaluated analytically through the singularity like Ref. [15]. However, in this work, not all contributions of the induced electric currents in the dominant region ($\boldsymbol{J}_{1_\mathrm{l}}$, $\boldsymbol{J}_{1_\mathrm{r}}$ and $\boldsymbol{J}_\mathrm{o}$) were considered. $\boldsymbol{J}_{2_\mathrm{l}}$ and $\boldsymbol{J}_{2_\mathrm{r}}$ depend mainly on the incident magnetic field $\boldsymbol{H}_{2_\mathrm{l}}^{\mathrm{inc}}(\boldsymbol{r})$ or $\boldsymbol{H}_{2_\mathrm{r}}^{\mathrm{inc}}(\boldsymbol{r})$ and $\boldsymbol{J}_{1_\mathrm{l}}$ or $\boldsymbol{J}_{1_\mathrm{r}}$ in the dominant region.

For the HH polarization, applying the MOM to the dominant region, and substituting Eqs. (7) , (8), and (3) into (1), the matrix equation of EM scattering from a PEC rough surface can be written as

$$\hat{\boldsymbol{t}} \cdot \begin{bmatrix} \bar{\boldsymbol{A}}_{11} & \bar{\boldsymbol{A}}_{12} \\ \bar{\boldsymbol{A}}_{21} & \bar{\boldsymbol{A}}_{22} \end{bmatrix} \cdot \begin{bmatrix} \boldsymbol{J}_{1_\mathrm{l}} \\ \boldsymbol{J}_{1_\mathrm{r}} \end{bmatrix} = \hat{\boldsymbol{t}} \cdot \begin{bmatrix} \boldsymbol{b}_1 \\ \boldsymbol{b}_2 \end{bmatrix}, \quad (9)$$

and

$$\begin{aligned}
&\bar{\boldsymbol{A}}_{11} = \bar{\boldsymbol{L}}_\mathrm{E}^{1_\mathrm{l}1_\mathrm{l}} + \bar{\boldsymbol{L}}_\mathrm{E}^{1_\mathrm{l}2_\mathrm{l}} \cdot 2\hat{\boldsymbol{n}} \times \bar{\boldsymbol{L}}_\mathrm{H}^{2_\mathrm{l}1_\mathrm{l}}, \\
&\bar{\boldsymbol{A}}_{22} = \bar{\boldsymbol{L}}_\mathrm{E}^{1_\mathrm{r}1_\mathrm{r}} + \bar{\boldsymbol{L}}_\mathrm{E}^{1_\mathrm{r}2_\mathrm{r}} \cdot 2\hat{\boldsymbol{n}} \times \bar{\boldsymbol{L}}_\mathrm{H}^{2_\mathrm{r}1_\mathrm{r}}, \\
&\bar{\boldsymbol{A}}_{12} = \bar{\boldsymbol{L}}_\mathrm{E}^{1_\mathrm{l}1_\mathrm{r}}, \quad \bar{\boldsymbol{A}}_{21} = \bar{\boldsymbol{L}}_\mathrm{E}^{1_\mathrm{r}1_\mathrm{l}}, \\
&\boldsymbol{b}_1 = \boldsymbol{E}_{1_\mathrm{l}}^{\mathrm{inc}} + \bar{\boldsymbol{L}}_\mathrm{E}^{1_\mathrm{l}2_\mathrm{l}} \cdot 2\hat{\boldsymbol{n}} \times \boldsymbol{H}_{2_\mathrm{l}}^{\mathrm{inc}}, \\
&\boldsymbol{b}_2 = \boldsymbol{E}_{1_\mathrm{r}}^{\mathrm{inc}} + \bar{\boldsymbol{L}}_\mathrm{E}^{1_\mathrm{r}2_\mathrm{r}} \cdot 2\hat{\boldsymbol{n}} \times \boldsymbol{H}_{2_\mathrm{r}}^{\mathrm{inc}}.
\end{aligned}$$

If a target is located above the rough surface, the matrix equation will be

$$\hat{\boldsymbol{t}} \cdot \begin{bmatrix} \bar{\boldsymbol{A}}_{11} & \bar{\boldsymbol{A}}_{12} & \bar{A}_{13} \\ \bar{\boldsymbol{A}}_{21} & \bar{\boldsymbol{A}}_{22} & \bar{A}_{23} \\ \bar{\boldsymbol{A}}_{31} & \bar{\boldsymbol{A}}_{32} & \bar{A}_{33} \end{bmatrix} \cdot \begin{bmatrix} \boldsymbol{J}_{1_\mathrm{l}} \\ \boldsymbol{J}_{1_\mathrm{r}} \\ \boldsymbol{J}_\mathrm{o} \end{bmatrix} = \hat{\boldsymbol{t}} \cdot \begin{bmatrix} \boldsymbol{b}_1 \\ \boldsymbol{b}_2 \\ \boldsymbol{b}_3 \end{bmatrix}, \quad (10)$$

where $\bar{\boldsymbol{A}}_{11}$, $\bar{\boldsymbol{A}}_{12}$, $\bar{\boldsymbol{A}}_{21}$, $\bar{\boldsymbol{A}}_{22}$, $\boldsymbol{b}_1$ and $\boldsymbol{b}_2$ are the same as those in Eq. (9). The other elements are $\bar{\boldsymbol{A}}_{13} = \bar{\boldsymbol{L}}_\mathrm{E}^{1_\mathrm{lo}}$, $\bar{\boldsymbol{A}}_{23} = \bar{\boldsymbol{L}}_\mathrm{E}^{2_\mathrm{lo}}$, $\bar{\boldsymbol{A}}_{31} = \bar{\boldsymbol{L}}_\mathrm{E}^{\mathrm{o}1_\mathrm{l}}$, $\bar{\boldsymbol{A}}_{32} = \bar{\boldsymbol{L}}_\mathrm{E}^{\mathrm{o}1_\mathrm{r}}$, $\bar{\boldsymbol{A}}_{33} = \bar{\boldsymbol{L}}_\mathrm{E}^{\mathrm{oo}}$ and $\boldsymbol{b}_3 = \boldsymbol{E}_\mathrm{o}^{\mathrm{inc}}$. Please note that in the subscripts

and the superscript, o represents object which is located above the rough surface. It is the same for the following variables.

For the VV polarization, the matrix equation of EM scattering from a PEC rough surface is

$$\begin{bmatrix} \bar{\boldsymbol{A}}_{11} & \bar{\boldsymbol{A}}_{12} \\ \bar{\boldsymbol{A}}_{21} & \bar{\boldsymbol{A}}_{22} \end{bmatrix} \cdot \begin{bmatrix} \boldsymbol{J}_{1_\mathrm{l}} \\ \boldsymbol{J}_{1_\mathrm{r}} \end{bmatrix} = \begin{bmatrix} \boldsymbol{b}_1 \\ \boldsymbol{b}_2 \end{bmatrix} \tag{11}$$

where

$$\begin{aligned}
&\bar{\boldsymbol{A}}_{11} = 1 - \hat{\boldsymbol{n}} \times (\bar{\boldsymbol{L}}_{\mathrm{H}}^{1_\mathrm{l}1_\mathrm{l}} + \bar{\boldsymbol{L}}_{\mathrm{H}}^{1_\mathrm{l}2_\mathrm{l}} \cdot 2\hat{\boldsymbol{n}} \times \bar{\boldsymbol{L}}_{\mathrm{H}}^{2_\mathrm{l}1_\mathrm{l}}),\\
&\bar{\boldsymbol{A}}_{22} = 1 - \hat{\boldsymbol{n}} \times (\bar{\boldsymbol{L}}_{\mathrm{H}}^{1_\mathrm{r}1_\mathrm{r}} + \bar{\boldsymbol{L}}_{\mathrm{H}}^{1_\mathrm{r}2_\mathrm{r}} \cdot 2\hat{\boldsymbol{n}} \times \bar{\boldsymbol{L}}_{\mathrm{H}}^{2_\mathrm{r}1_\mathrm{r}}),\\
&\bar{\boldsymbol{A}}_{12} = \bar{\boldsymbol{L}}_{\mathrm{H}}^{1_\mathrm{l}1_\mathrm{r}}, \quad \bar{\boldsymbol{A}}_{21} = \bar{\boldsymbol{L}}_{\mathrm{H}}^{1_\mathrm{r}1_\mathrm{l}},\\
&\boldsymbol{b}_1 = \hat{\boldsymbol{n}} \times (\boldsymbol{H}_{1_\mathrm{l}}^{\mathrm{inc}} + \bar{L}_{\mathrm{H}}^{1_\mathrm{l}2_\mathrm{l}} \cdot 2\hat{\boldsymbol{n}} \times \boldsymbol{H}_{2_\mathrm{l}}^{\mathrm{inc}}),\\
&\boldsymbol{b}_2 = \hat{\boldsymbol{n}} \times (\boldsymbol{H}_{1_\mathrm{r}}^{\mathrm{inc}} + \bar{\boldsymbol{L}}_{\mathrm{H}}^{1_\mathrm{r}2_\mathrm{r}} \cdot 2\hat{\boldsymbol{n}} \times \boldsymbol{H}_{2_\mathrm{r}}^{\mathrm{inc}}).
\end{aligned}$$

If a target is located above the rough surface, the matrix equation will be

$$\begin{bmatrix} \bar{\boldsymbol{A}}_{11} & \bar{\boldsymbol{A}}_{12} & \bar{A}_{13} \\ \bar{\boldsymbol{A}}_{21} & \bar{\boldsymbol{A}}_{22} & \bar{A}_{23} \\ \bar{\boldsymbol{A}}_{31} & \bar{\boldsymbol{A}}_{32} & \bar{A}_{33} \end{bmatrix} \cdot \begin{bmatrix} \boldsymbol{J}_{1_\mathrm{l}} \\ \boldsymbol{J}_{1_\mathrm{r}} \\ \boldsymbol{J}_{\mathrm{o}} \end{bmatrix} = \begin{bmatrix} \boldsymbol{b}_1 \\ \boldsymbol{b}_2 \\ \boldsymbol{b}_3 \end{bmatrix}, \tag{12}$$

and $\bar{\boldsymbol{A}}_{11}$, $\bar{\boldsymbol{A}}_{12}$, $\bar{\boldsymbol{A}}_{21}$, $\bar{\boldsymbol{A}}_{22}$, $\boldsymbol{b}_1$ and $\boldsymbol{b}_2$ are the same as those in Eq. (11). The other elements are $\bar{\boldsymbol{A}}_{13} = \bar{\boldsymbol{L}}_{\mathrm{H}}^{1_\mathrm{lo}}$, $\bar{\boldsymbol{A}}_{23} = \bar{\boldsymbol{L}}_{\mathrm{H}}^{2_\mathrm{lo}}$, $\bar{\boldsymbol{A}}_{31} = \bar{\boldsymbol{L}}_{\mathrm{H}}^{\mathrm{o}1_\mathrm{l}}$, $\bar{\boldsymbol{A}}_{32} = \bar{\boldsymbol{L}}_{\mathrm{H}}^{\mathrm{o}1_\mathrm{r}}$, $\bar{\boldsymbol{A}}_{33} = \bar{\boldsymbol{L}}_{\mathrm{H}}^{\mathrm{oo}}$ and $\boldsymbol{b}_3 = \boldsymbol{H}_{\mathrm{o}}^{\mathrm{inc}}$.

From the above four equations, it is readily seen that contributions of the induced electric currents $\boldsymbol{J}_{3_\mathrm{l}}, \ldots, \boldsymbol{J}_{M_\mathrm{r}}$ on regions $S_{3_\mathrm{l}}, \ldots, S_{M_\mathrm{r}}$ are neglected. That is because the induced electric current in the edge of the rough surface is very smaller than that in the center. Regions $S_{3_\mathrm{l}}, \ldots, S_{M_\mathrm{r}}$ are far away from regions S_{1_l} or S_{1_r}. Electric currents $\boldsymbol{J}_{3_\mathrm{l}}, \ldots, \boldsymbol{J}_{M_\mathrm{r}}$ are much smaller than $\boldsymbol{J}_{1_\mathrm{l}}$ or $\boldsymbol{J}_{1_\mathrm{r}}$. Another point worth noting is that the MOM is only adopted in the dominant region (S_{1_l}, S_{1_r} and S_{o}). Therefore, the number of unknowns of this approach can be greatly reduced comparing with the full MOM.

After the induced electric currents $\boldsymbol{J}_{1_\mathrm{l}}$, $\boldsymbol{J}_{1_\mathrm{r}}$ and $\boldsymbol{J}_{\mathrm{o}}$ in the dominant region are obtained, electric currents $\boldsymbol{J}_{2_\mathrm{l}}$ and $\boldsymbol{J}_{2_\mathrm{r}}$ can be achieved through Eqs. (7) and (8), respectively. Furthermore, the electric currents $\boldsymbol{J}_{3_\mathrm{l}}$ and $\boldsymbol{J}_{3_\mathrm{r}}$ can be acquired as

$$\begin{aligned}
\boldsymbol{J}_{3_\mathrm{l}}(\boldsymbol{r}) &= 2\hat{\boldsymbol{n}} \times \boldsymbol{H}_{3_\mathrm{l}}^{\mathrm{inc}}(\boldsymbol{r}) + 2\hat{\boldsymbol{n}} \times \bar{\boldsymbol{L}}_{\mathrm{H}}^{3_\mathrm{l}1_\mathrm{l}} \cdot \boldsymbol{J}_{1_\mathrm{l}} \\
&\quad + 2\hat{n} \times \bar{\boldsymbol{L}}_{\mathrm{H}}^{3_\mathrm{l}2_\mathrm{l}} \cdot \boldsymbol{J}_{2_\mathrm{l}}, \qquad (13)\\
\boldsymbol{J}_{3_\mathrm{r}}(\boldsymbol{r}) &= 2\hat{\boldsymbol{n}} \times \boldsymbol{H}_{3_\mathrm{r}}^{\mathrm{inc}}(\boldsymbol{r}) + 2\hat{\boldsymbol{n}} \times \bar{\boldsymbol{L}}_{\mathrm{H}}^{3_\mathrm{r}1_\mathrm{r}} \cdot \boldsymbol{J}_{1_\mathrm{r}} \\
&\quad + 2\hat{n} \times \bar{\boldsymbol{L}}_{\mathrm{H}}^{3_\mathrm{r}2_\mathrm{r}} \cdot \boldsymbol{J}_{2_\mathrm{r}}. \qquad (14)
\end{aligned}$$

In which, contributions of the induced electric currents $\boldsymbol{J}_{4_\mathrm{l}}, \ldots, \boldsymbol{J}_{M_\mathrm{r}}$ in regions $S_{4_\mathrm{l}}, \ldots, S_{M_\mathrm{r}}$ are neglected. In general, the electric currents $\boldsymbol{J}_{m_\mathrm{l}}$ and $\boldsymbol{J}_{m_\mathrm{r}}$ can be obtained as

$$\begin{aligned}
\boldsymbol{J}_{m_\mathrm{l}}(\boldsymbol{r}) &= 2\hat{\boldsymbol{n}} \times \boldsymbol{H}_{m_\mathrm{l}}^{\mathrm{inc}}(\boldsymbol{r}) \\
&\quad + \sum_{p=1}^{m-1} 2\hat{\boldsymbol{n}} \times \bar{\boldsymbol{L}}_{\mathrm{H}}^{m_\mathrm{l}p_\mathrm{l}} \cdot \boldsymbol{J}_{p_\mathrm{l}}, \qquad (15)\\
\boldsymbol{J}_{m_\mathrm{r}}(\boldsymbol{r}) &= 2\hat{\boldsymbol{n}} \times \boldsymbol{H}_{m_\mathrm{r}}^{\mathrm{inc}}(\boldsymbol{r}) \\
&\quad + \sum_{p=1}^{m-1} 2\hat{\boldsymbol{n}} \times \bar{\boldsymbol{L}}_{\mathrm{H}}^{m_\mathrm{r}p_\mathrm{r}} \cdot \boldsymbol{J}_{p_\mathrm{r}}, \qquad (16)
\end{aligned}$$

where $m = 3, \ldots, M$. It is necessary to note that the new model is an approximate method, and has an advantage of greatly reducing the number of unknowns.

In this work, the tapered plane wave was chosen as the incident wave to avoid the artificial edge diffraction resulting from finite length of the simulated rough surface. For HH polarization, the incident electric field is[16]

$$\begin{aligned}
\boldsymbol{E}^{\mathrm{inc}}(\boldsymbol{r}) &= \hat{\boldsymbol{y}}\varphi^{\mathrm{inc}}(\boldsymbol{r}) \\
&= \hat{\boldsymbol{y}} \exp(\mathrm{i}\, k_0(x\sin\theta_{\mathrm{i}} - z\cos\theta_{\mathrm{i}})(1 + w(\boldsymbol{r}))) \\
&\quad \times \exp\left(- \frac{(x + z\tan\theta_{\mathrm{i}})^2}{g^2} \right), \qquad (17)
\end{aligned}$$

where $w(\boldsymbol{r}) = [2(x + z\tan\theta_{\mathrm{i}})^2/g^2 - 1]/(k_0 g\cos\theta_{\mathrm{i}})^2$, θ_{i} is the incident angle defined with respect to the normal vector in the counterclockwise direction, g is the tapering parameter. Then the incident magnetic field is

$$\begin{aligned}
\boldsymbol{H}^{\mathrm{inc}}(\boldsymbol{r}) &= \frac{\mathrm{i}}{\omega\mu_0}\{\hat{\boldsymbol{x}}\varphi^{\mathrm{inc}}(\boldsymbol{r})[P_1 + \tan\theta_{\mathrm{i}} P_2] \\
&\quad - \hat{\boldsymbol{z}}\varphi^{\mathrm{inc}}(\boldsymbol{r})[P_3 + P_2]\}, \qquad (18)
\end{aligned}$$

and

$$\begin{aligned}
P_1 &= -\mathrm{i}\, k_0\cos\theta_{\mathrm{i}}(1 + w(\boldsymbol{r})),\\
P_2 &= 2(x + z\tan\theta_{\mathrm{i}}) \\
&\quad \times [\mathrm{i}\, 2k_0(x\sin\theta_{\mathrm{i}} - z\cos\theta_{\mathrm{i}})/(k_0 g\cos\theta_{\mathrm{i}})^2 - 1]/g^2,\\
P_3 &= \mathrm{i}\, k_0\sin\theta_{\mathrm{i}}(1 + w(\boldsymbol{r})).
\end{aligned}$$

For VV polarized incident wave, the incident magnetic field is[16]

$$\begin{aligned}
\boldsymbol{H}^{\mathrm{inc}}(\boldsymbol{r}) &= \hat{\boldsymbol{y}}\varphi^{\mathrm{inc}}(\boldsymbol{r}) \\
&= \hat{\boldsymbol{y}} \exp(\mathrm{i}\, k_0(x\sin\theta_{\mathrm{i}} - z\cos\theta_{\mathrm{i}})(1 + w(\boldsymbol{r}))) \\
&\quad \times \exp\left(- \frac{(x + z\tan\theta_{\mathrm{i}})^2}{g^2} \right). \qquad (19)
\end{aligned}$$

In the observational direction with $\boldsymbol{k}_{\rm s} = k_0(\hat{\boldsymbol{x}}\sin\theta_{\rm s} + \hat{\boldsymbol{z}}\cos\theta_{\rm s})$, the BSC is defined as the same as that given in Ref. [16]

$$\sigma(\theta_{\rm s}) = \frac{|\psi_{\rm s}^{(N)}(\theta_{\rm s})|^2}{8\pi k_0 g\sqrt{\frac{\pi}{2}}\cos\theta_{\rm i}\left[1-\frac{1+2\tan^2\theta_{\rm i}}{2(k_0 g\cos\theta_{\rm i})^2}\right]}, \quad (20)$$

where for HH polarization

$$\psi_{\rm s}^{(N)}(\theta_{\rm s}) = {\rm i}\,k_0\eta\int_S J(\boldsymbol{r}')\exp(-{\rm i}\,k_0\boldsymbol{r}'\cdot\hat{\boldsymbol{R}}){\rm d}S, \quad (21)$$

and, $\boldsymbol{r}' = x\hat{\boldsymbol{x}} + f(x)\hat{\boldsymbol{z}}$, $\hat{\boldsymbol{R}} = \sin\theta_{\rm s}\hat{\boldsymbol{x}} + \cos\theta_{\rm s}\hat{\boldsymbol{z}}$. For VV polarization

$$\psi_{\rm s}^{(N)}(\theta_{\rm s}) = -{\rm i}\,k_0\int_S J(\boldsymbol{r}')\hat{\boldsymbol{n}}\cdot\hat{\boldsymbol{R}} \times\exp(-{\rm i}\,k_0\boldsymbol{r}'\cdot\hat{\boldsymbol{R}}){\rm d}S. \quad (22)$$

3. Numerical simulations and discussion

Firstly, to ensure the validity of the presented approach, EM scattering from a PEC Gaussian rough surface was calculated by the multiregion model (multi-MOM) and full MOM, respectively. HH and VV polarizations were both considered. In Table 1, the simulating time of the two different methods is provided for one same-surface realization, which includes three parts: filling the impedance matrix, solving the matrix equation and the total time. Here, the Gaussian rough surface is divided into $N = 1024$ segments with $\Delta x = \lambda/10$, which represents a simulated length of $L = 102.4\lambda$. The rms height and correlation length are $\delta = 0.2\lambda$, $l = \lambda$. In this calculation, parameters of the incident tapered wave were given by $\lambda = 0.1$ m, $\theta_{\rm i} = 30^\circ$, and $g = L/4$. To perform the multiregion model, the rough surface was divided into four regions with unknowns $N_{1_{\rm l}} = 256$, $N_{1_{\rm r}} = 256$, $N_{2_{\rm l}} = 256$ and $N_{2_{\rm r}} = 256$. Hence, the number of unknowns in the new model is only 50% of that in the full MOM. From Table 1, it is obvious that solving time of the multi-MOM is about 25% of the full MOM. The total time of the multi-MOM is also less than that of the full MOM. Another point worth noting is that filling the impedance matrix of the multi-MOM is more time-consuming than that of the full MOM. We attribute this result to the fact that the operators $\bar{\boldsymbol{L}}_{\rm E}^{mn}\cdot 2\hat{\boldsymbol{n}}\times\bar{\boldsymbol{L}}_{\rm H}^{nm}$ and $\bar{\boldsymbol{L}}_{\rm H}^{mn}\cdot 2\hat{\boldsymbol{n}}\times\bar{\boldsymbol{L}}_{\rm H}^{nm}$ of the multi-MOM have twice matrix-vector products. Thus, if a fast algorithm, such as the fast multiple method,[20] is applied to compute the matrix-vector product, the efficiency of the new model can be greatly improved.

Table 1. Simulating time of the multi-MOM and full MOM for one same-surface realization.

Polarization	Method	Number of unknowns	Filling time/s	Solving time/s	Total time/s
HH	full MOM	1024	0.6875	2.125	2.875
	multi-MOM	512	0.9844	0.5625	1.5938
VV	full MOM	1024	1.0938	1.8125	2.9844
	multi-MOM	512	1.6563	0.4531	2.1719

Figure 3 shows the comparison of the present calculations with the full MOM calculations for the distribution of the induced electric current along the one rough surface realization for both HH and VV polarization. It can be seen that the electric currents in the dominant region obtained by the two different methods are in fairly good agreement, but there is an obvious discrepancy in the right margin of the rough surface, especially for HH polarization. This inconsistency should be particularly surprising, the primary reason for this is due to the fact that the contributions of $\boldsymbol{J}_{2_{\rm l}}$ and $\boldsymbol{J}_{1_{\rm l}}$ to $\boldsymbol{J}_{2_{\rm r}}$ have been neglected in the numerical simulations and these contributions have less influence on the result at the VV polarization. For the induced electric current along the tangential direction $\hat{\boldsymbol{t}}$, $\boldsymbol{J}_{2_{\rm r}}$ depends more on the electric current of its close neighbour ($\boldsymbol{J}_{1_{\rm r}}$) at this case.

In Fig. 4, the angular distribution of the BSC obtained by the two methods is presented by averaging 50 Monte Carlo realizations. From Fig. 4, it is readily observed that the BSC of the multi-MOM is in good agreement with the full MOM over the whole scattering angle for the VV polarization. However, there is an apparent discrepancy for the BSC at the larger scattering angle region for the HH case. From the geometric model of this scattering problem in Fig. 1,

one can conclude that the BSC at the larger scattering angle region depends more on the electric current at the edge of the rough surface. The discrepancy of the electric current in the right margin of the rough surface (Fig. 3) causes the difference of the BSC at the larger scattering angle region (Fig. 4). Another point worth noting is that the amplitude of the electric current is much smaller for the HH polarization, a much smaller discrepancy of the electric current can lead to a large visible change on the BSC at the larger scattering angle region. The results of Figs. 3 and 4 demonstrate the validity and accuracy of the multi-region model presented in this paper for calculating EM scattering from a PEC rough surface, especially for small and moderate scattering angles.

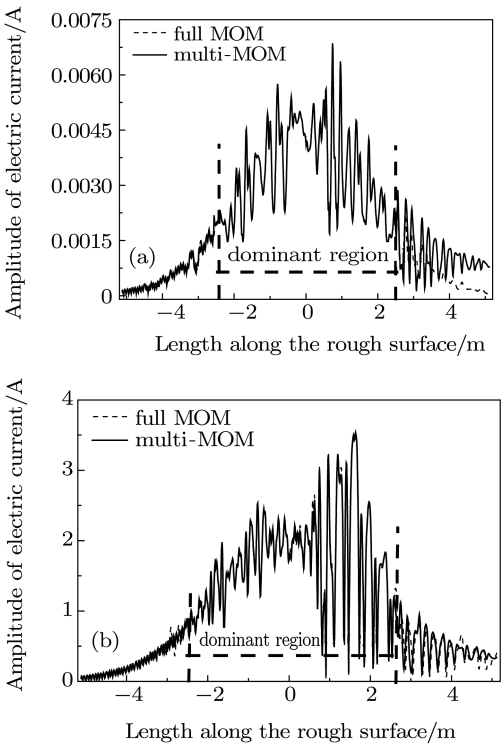


Fig. 3. Comparisons of the induced electric current along the rough surface by multi-MOM and full MOM. (a) HH polarization, (b) VV polarization.

To further validate the presented approach in computing the EM scattering from a PEC rough surface with a target above it, in the next simulations, a PEC cylinder or a PEC square above a Gaussian rough surface were considered. A cylinder ($r = 2\lambda$, $h = 5\lambda$, $N_{\rm o} = 160$) or a square ($r = 4\lambda$, $h = 5\lambda$, $N_{\rm o} = 160$) was located above a Gaussian rough surface ($L = 204.8\lambda$, $\Delta x = \lambda/10$) as shown in Fig. 5. The Gaussian rough surface was divided into six segments with $N_{1_l} = 256$, $N_{1_r} = 256$, $N_{2_l} = 256$, $N_{2_r} = 256$, $N_{3_l} = 512$ and $N_{3_r} = 512$. Hence, the number of unknowns in the new model was about 30% of that in the full MOM. The parameters of the tapered wave were still given by $\lambda = 0.1$ m and $g = L/4$.

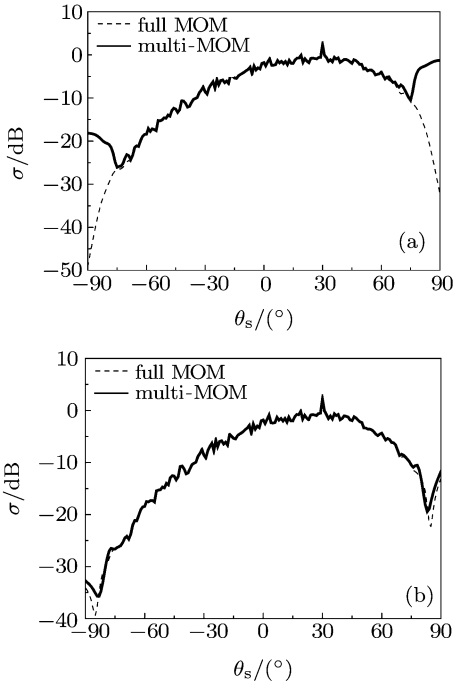


Fig. 4. Comparisons of the BSC from a PEC Gaussian rough surface by the multi-MOM and full MOM. (a) HH polarization, (b) VV polarization.

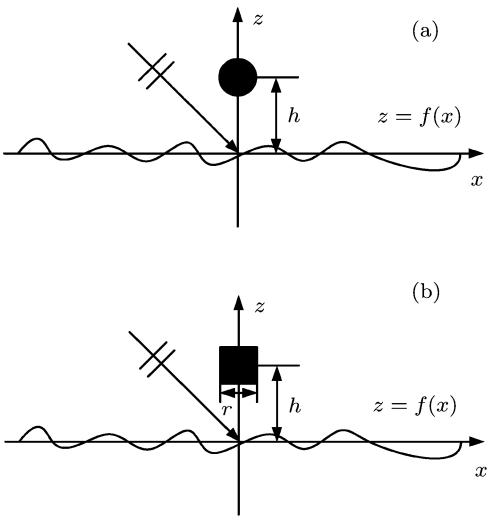


Fig. 5. (a) Geometry of EM scattering from a cylinder located above a Gaussian rough surface, (b) geometry of EM scattering from a square located above a Gaussian rough surface.

The scattering behaviour of a cylinder located above a Gaussian rough surface with an incident angle of $\theta_{\rm i} = 45^\circ$ was firstly taken into account, in which

the rms height and correlation length of the Gaussian rough surface were set to be $\delta = 0.2\lambda$, $l = \lambda$, respectively. A comparison of the simulating time by the multi-MOM and the full method of moments is exhibited in Table 2 for one same-composite realization. The filling, the solving and the total times are also presented in Table 2. As can be seen in Table 2, the total time of the multi-MOM is 12.82% at HH polarization and 12.34% at VV polarization of those by the full method of moments. From Table 2, it is also found that solving the matrix equation of the full method of moments is more time-consuming than the multi-MOM for the larger number of unknowns.

Table 2. The simulating time of the multi-MOM and the full MOM for one same-composite realization.

Polarization	Method	Number of unknowns	Filling time/s	Solving time/s	Total time/s
HH	full MOM	2208	2.5469	9.5625	12.1875
	multi-MOM	672	0.6875	0.7969	1.5625
VV	full MOM	2208	2.7969	11.4375	14.3125
	multi-MOM	672	0.7188	0.9688	1.7656

The distribution of induced electric current along the rough surface is depicted in Fig. 6 for one composite realization. It is necessary to point out that the interactions between the rough surface and the cylinder were considered. The electric current depends not only on the incident taper wave but also on the scattered field of the cylinder. Similar to the illustration in Fig. 3, it is also seen that the electric currents in the dominant region are almost the same for the two different methods. There is also an evident discrepancy in regions far away from the dominant region, which results from that the induced electric current is obtained approximately by considering the mutual coupling between different regions along the rough surface and that several contributions of the induced electric currents are neglected.

In Fig. 7, the induced electric currents along the cylinder are presented for both HH and VV polarization. All contributions of the incident taper wave and the scattered filed from the Gaussian rough surface are considered. From Fig. 7, it is observed that the same results are achieved through the two different methods. The primary reason for the

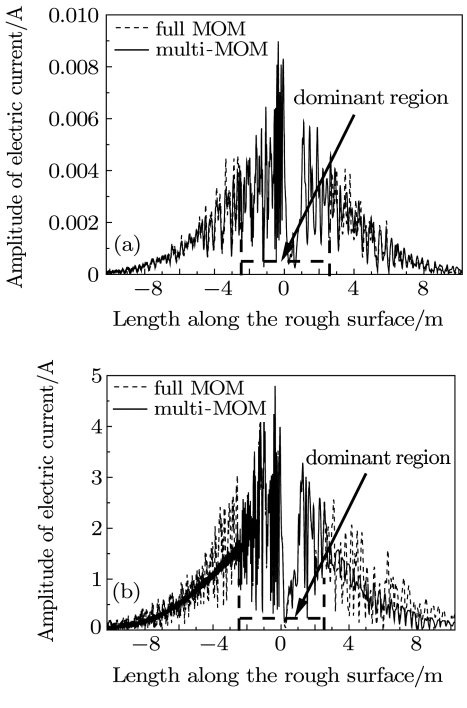


Fig. 6. Comparisons of the induced electric current along the Gaussian rough surface. (a) HH polarization, (b) VV polarization.

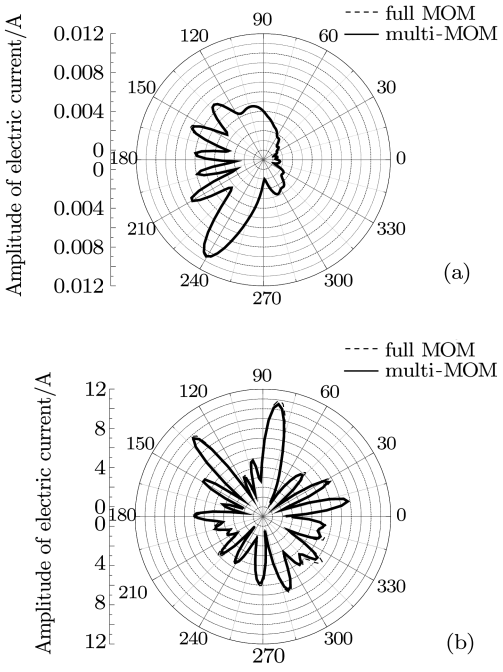


Fig. 7. Comparisons of the induced electric current along the cylinder. (a) HH polarization, (b) VV polarization.

consistency is that the cylinder is distributed into the dominant region and dealt with by the MOM in this multiregion model. In other words, the validity of this approach is ensured through the MOM adopted on the dominant region. The number of unknowns can be significantly reduced by only applying the MOM in the dominant region.

The scattering pattern of the BSC from this composite model is shown in Fig. 8 by averaging 50 surface realizations. It can be easily seen that the two methods are in fairly good agreement, especially for small and moderate scattering angles. However, an obvious discrepancy appears in the large scattering angle region for HH polarization, the reason for this is similar to the explanation for the rough surface scattering presented in Fig. 4(a), i.e., the amplitude of the electric current is much smaller for HH polarization, and the discrepancy of the electric current causes the apparent difference in the large scattering angles. Hence, the presented multiregion model is also valid for computing the EM scattering from a cylinder located above a Gaussian rough surface, particularly for small and moderate scattering angles.

The scattering behaviour of a square located above a Gaussian rough surface has been examined, where the rms height and correlation length were $\delta = 0.5\lambda$, $l = 1.5\lambda$, and the incident angle was $\theta_{\rm i} = 45°$. The simulating time from this composite model obtained by the multi-MOM and the full MOM is also presented in Table 3. The superiority of the multi-MOM is more obvious in this condition. The total time of the multi-MOM is about 8.19% at HH polarization and 4.53% at VV polarization of that of full MOM.

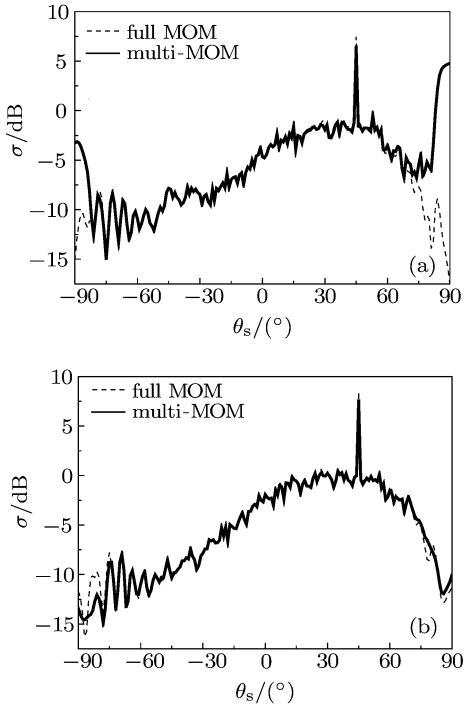


Fig. 8. Comparisons of the BSC from a cylinder located above a PEC Gaussian rough surface. (a) HH polarization, (b) VV polarization.

Table 3. The simulating time of the multi-MOM and the full MOM for one same-composite realization.

Polarization	Method	Number of unknowns	Filling time/s	Solving time/s	Total time/s
HH	full MOM	2208	3.3906	35.7969	39.2969
	multi-MOM	672	1.125	1.9688	3.2188
VV	full MOM	2208	4.75	126.875	131.75
	multi-MOM	672	1.3281	4.5156	5.9688

The distribution of the induced electric current along the rough surface is illustrated in Fig. 9, where the interaction between the rough surface and the square are considered. The angular distribution of the BSC is also exhibited in Fig. 10. Similar to the analysis in Fig. 3 and Fig. 6, the electric currents show good agreement in the dominant region by both the multi-MOM and the full MOM. The electric current in other regions are achieved by approximately considering the mutual coupling, which causes an obvious discrepancy of the electric current in these regions and an apparent difference of the BSC in the large scattering angles for HH polarization. From Fig. 10, one can also conclude that the BSC of the new model shows good agreement with the full MOM at VV polarization. The validity of the presented multiregion model, particularly for small and moderate scattering angles, is also exhibited in these results for a square located above a Gaussian rough surface.

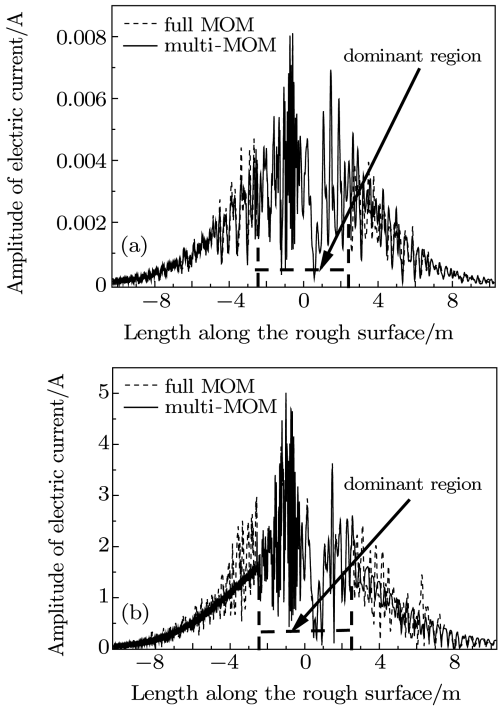


Fig. 9. Comparisons of the induced electric current along the Gaussian rough surface. (a) HH polarization, (b) VV polarization.

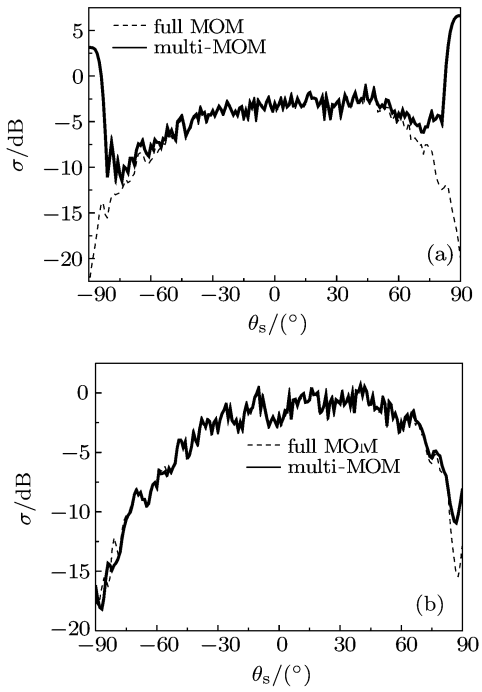


Fig. 10. Comparisons of the BSC from a square located above a PEC Gaussian rough surface. (a) HH polarization, (b) VV polarization.

Finally, the validity of the presented algorithm under larger incidence was also implemented for both HH and VV polarizations. A cylinder ($r = 2\lambda$, $h = 5\lambda$, $N_{\rm o} = 160$) was located above a Gaussian rough surface ($L = 819.2\lambda$, $\Delta x = \lambda/10$, $\delta = 0.2\lambda$, $l = \lambda$) with the incident wave ($\lambda = 0.1$ m, $g = L/4$, $\theta_{\rm i} = 80°$). The Gaussian rough surface was also divided into six segments with $N_{1_{\rm l}} = 1024$, $N_{1_{\rm r}} = 1024$, $N_{2_{\rm l}} = 1024$, $N_{2_{\rm r}} = 1024$, $N_{3_{\rm l}} = 2048$ and $N_{3_{\rm r}} = 2048$. Therefore, the number of unknowns in this new model is about 30% of that in the full MOM.

The simulating times of the multi-MOM and the full MOM under the larger incidence are shown in Table 4, respectively. It can be obviously seen that the multi-MOM is more efficient than the full MOM. The solving time of the multi-MOM is only 2% of that of the full MOM. In addition, the total time of the multi-MOM is 14.68% with HH polarization and 13.71% at VV polarization. From this table, it can be also seen that filling the impedance matrix of the multi-MOM is more time-consuming for the operators $\bar{\boldsymbol{L}}_{\rm E}^{mn} \cdot 2\hat{\boldsymbol{n}} \times \bar{\boldsymbol{L}}_{\rm H}^{nm}$ and $\bar{\boldsymbol{L}}_{\rm H}^{mn} \cdot 2\hat{\boldsymbol{n}} \times \bar{\boldsymbol{L}}_{\rm H}^{nm}$.

Table 4. The simulating time of the multi-MOM and the full MOM for one same-composite realization.

Polarization	Method	Number of unknowns	Filling time/s	Solving time/s	Total time/s
HH	full MOM	8352	34.22	1086.17	1120.67
	multi-MOM	2208	144.5	19.70	164.51
VV	full MOM	8352	40.0	1192.34	1232.61
	multi-MOM	2208	149.20	19.48	168.97

The induced electric current along the cylinder is depicted in Fig. 11, where the interactions between the rough surface and the cylinder are considered. From this figure, a small difference is observed for HH polarization. The two patterns of the multi-MOM and the full MOM overlay each other very well at VV polarization. The bistatic scattering patterns under larger incidence obtained by the multi-MOM and full MOM

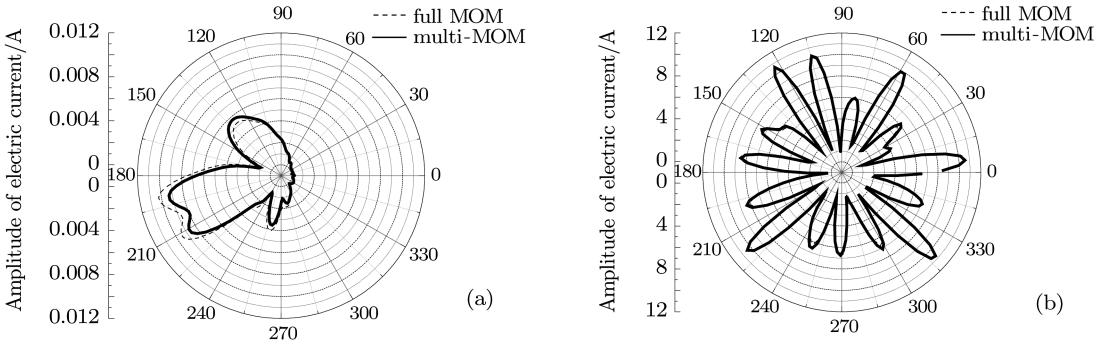


Fig. 11. Comparisons of the induced electric current along the cylinder under larger incidence. $\theta_{\rm i} = 80°$. (a) HH polarization, (b) VV polarization.

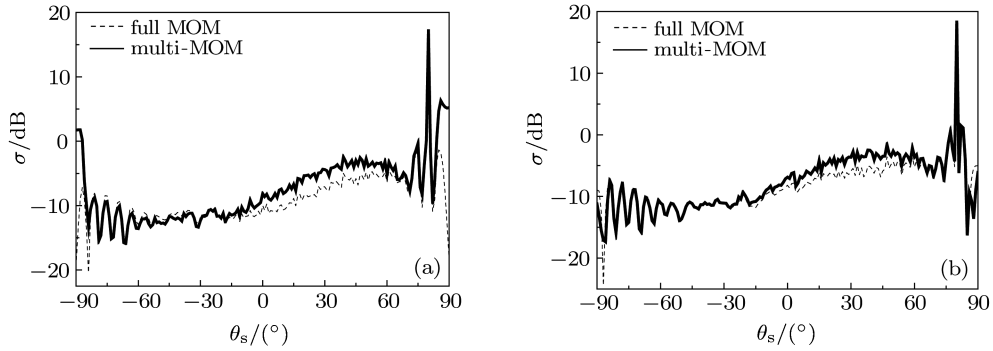


Fig. 12. Comparisons of the BSC from a cylinder above a Gaussian rough surface under larger incidence. $\theta_{\rm i} = 80°$. (a) HH polarization, (b) VV polarization.

are also provided in Fig. 12. It can be easily seen that the BSC of the multi-MOM shows a good agreement with the full MOM over the most scattering regions under the VV polarization. There is also an obvious discrepancy for the larger scattering angles at the HH case, but there is good coincidence in the specular direction. In general, the presented multiregion model is valid for computing EM scattering under larger incidence.

4. Conclusion

In this study, an efficient multiregion model is introduced to calculate EM scattering from a Gaussian rough surface with or without a target above it for both HH and VV polarizations. The rough surface was split into multiple regions, depending on their position along the rough surface, and the two intermediate regions was the dominant region handled by the MOM to ensure validity. Therefore, the multiregion model can greatly reduce the number of unknowns of the full MOM. If a target is located above the rough surface, the target will also be included in the dominant region. The validity and accuracy of the presented approach is shown by comparing it with the full MOM, including the distributions of the induced current along the rough surface and the angular distribution of the BSC. It is necessary to note that the amplitude of the electric current at HH polarizatiob is much smaller and that the electric current, except for the dominant regions, is obtained by approximately considering the mutual coupling between different regions along the rough surface. As a result, there is an apparent difference of BSC in the large scattering angles for the HH polarization. The EM scattering from a 2D rough surface or a dielectric rough surface with and without a target will be calculated by the approach in future. In addition, fast and advanced methods such as the BMIA/CAG,[9] the GFBM/SAA,[10] the MSMCG[11] and the fast multiple method[20] will be combined with the multiregion model to improve computing efficiency.

References

[1] Ma J, Guo L X and Wang A Q 2009 *Chin. Phys.* B **18** 3431

[2] Wang R, Guo L X and Ma J 2009 *Chin. Phys.* B **18** 3422

[3] Yang C, Guo L X and Wu Z S 2010 *Chin. Phys.* B **19** 054101

[4] Thorsos E I 1988 *Journal of Acoustical Society of American* **83** 78

[5] Zhang Y, Yang Y E, Braunisch H and Kong J A 1999 *Progress in Electromagnetics Research* **22** 315

[6] Li J, Guo L X and Zeng H 2008 *Waves in Random and Complex Media* **18** 641

[7] Guo L X, Wang A Q and Ma J 2009 *Progress in Electromagnetics Research* **89** 149

[8] Wang X, Wang C F, Gan Y B and Li L W 2003 *Progress in Electromagnetics Research* **40** 207

[9] Tsang L, Chan C H, Pak K and Sangani H 1995 *IEEE Trans. Antennas Propag.* **43** 851

[10] Li Z X and Jin Y Q 2001 *Microwave Opt. Technol. Lett.* **31** 146

[11] Xia M Y, Chan C H, Li S Q, Zhang B and Tsang L 2003 *IEEE Trans. Antennas Propag.* **51** 1142

[12] Wang A Q, Guo L X and Chai C 2010 *J. Electromagnetic Waves and Applications* **24** 1315

[13] Wang R, Guo L X, Ma J and Wu Z S 2009 *Chin. Phys.* B **18** 1503

[14] Li J, Guo L X, Zeng H and Han X B 2009 *Chin. Phys.* B **18** 2757

[15] Cui T J, Lu W B, Qiao Z G, Hong W and Yin X X 2004 *IEEE Trans. Antennas Propag.* **52** 1707

[16] Tsang L, Kong J A and Ding K H 2001 *Scattering of Electromagnetic Wave* (New York: John Wiley & Sons. Inc)

[17] Ye H X and Jin Y Q 2007 *IEEE Trans. Geosci. Remote Sens.* **45** 1174

[18] Harrington R F 1993 *Filed Computation by Moment Method* (New York: IEEE Press)

[19] Tran P, Celli V and Maradudin A A 1994 *J. Opt. Soc. Am.* A **11** 1686

[20] Lu C C and Chew W C 1993 *IEE Proceedings*-H **140** 455